Computers, Materials & Continua

Tech Science Press

DOI: 10.32604/cmc.2023.043383

ARTICLE

An Efficient Method for Identifying Lower Limb Behavior Intentions Based on Surface Electromyography

Liuyi Ling[1,2,3], Yiwen Wang[1,*], Fan Ding[4], Li Jin[1], Bin Feng[3], Weixiao Li[3], Chengjun Wang[1] and Xianhua Li[1]

[1]School of Artificial Intelligence, Anhui University of Science and Technology, Huainan, 232001, China

[2]Institute of Environment-Friendly Materials and Occupational Health, Anhui University of Science and Technology, Wuhu, 241003, China

[3]School of Electrical & Information Engineering, Anhui University of Science and Technology, Huainan, 232001, China

[4]School of Mechanical Engineering, Anhui University of Science and Technology, Huainan, 232001, China

*Corresponding Author: Yiwen Wang. Email: 2021201725@aust.edu.cn

Received: 30 June 2023 Accepted: 12 October 2023 Published: 26 December 2023

ABSTRACT

Surface electromyography (sEMG) is widely used for analyzing and controlling lower limb assisted exoskeleton robots. Behavior intention recognition based on sEMG is of great significance for achieving intelligent prosthetic and exoskeleton control. Achieving highly efficient recognition while improving performance has always been a significant challenge. To address this, we propose an sEMG-based method called Enhanced Residual Gate Network (ERGN) for lower-limb behavioral intention recognition. The proposed network combines an attention mechanism and a hard threshold function, while combining the advantages of residual structure, which maps sEMG of multiple acquisition channels to the lower limb motion states. Firstly, continuous wavelet transform (CWT) is used to extract signals features from the collected sEMG data. Then, a hard threshold function serves as the gate function to enhance signals quality, with an attention mechanism incorporated to improve the ERGN's performance further. Experimental results demonstrate that the proposed ERGN achieves extremely high accuracy and efficiency, with an average recognition accuracy of 98.41% and an average recognition time of only 20 ms-outperforming the state-of-the-art research significantly. Our research provides support for the application of lower limb assisted exoskeleton robots.

KEYWORDS

sEMG; movement intention; efficient network; convolutional neural network

1 Introduction

Surface electromyography (sEMG) is a bioelectrical signal generated by the human body, containing valuable information related to muscle activity. Signal processing is the process of converting raw sEMG signals into analyzable and applicable forms. By utilizing electromyography (EMG), predicting lower limb behavior intention can leverage the natural laws of human behavior for achieving human-machine interaction, facilitating seamless switching of robot working modes, improving robot

adaptability to the human body, and enhancing the overall experience of human-machine interaction. Furthermore, predicting human motion intention and recognizing motion posture have significant applications in many fields, for example, clinical analysis [1,2], healthcare [3,4], human-machine cooperation [5,6], virtual reality [7,8], bionic prosthesis [9,10].

In order to achieve exoskeleton control based on human motion intent accurately identifying such intent becomes crucial. At present, common methods for motion intention recognition mainly include force sensor based, inertial sensor based, visual sensor based, sEMG based, and electroencephalogram (EEG) based methods [11–16]. Among them, sEMG is a kind of biological electrical signal reflecting the activity of human superficial muscle, which has the advantages of non-invasiveness, high sensitivity, high timeliness and high correlation. sEMG is typically generated 30 to 150 ms prior to limb movements. This characteristic allows sEMG to predict behavior in advance or predict subsequent behavior. Research on behavioral intention recognition based on sEMG primarily focuses on this predictive capability and finds extensive application in gait analysis and robot control.

Due to the potential artifact interference and signal-to-noise ratio, the captured sEMG requires compression or enhancement through signal processing techniques to improve model prediction performance. Signal processing research has focused on denoising sEMG using methods such as empirical mode decomposition [17,18] and wavelet transform [19]. Other studies have concentrated on the feature extraction of signals. For example, Khushaba et al. proposed a feature extraction method for EMG based on spatio-temporal convolutions to improve the performance of existing electromyographic control systems [20]. Atzori et al. proposed a parallel window feature extractor (PaWFE) for extracting signal features in parallel from multiple time windows [21]. Furthermore, related traditional methods include linear discriminant analysis (LDA) [22], principal component analysis (PCA) [23], decision tree [24–27]. Deep learning algorithms have also been widely used in sEMG processing and behavioral intention recognition due to their ability to automatically learn data-representing features [28–32]. For instance, Wang et al. proposed an sEMG Gesture recognition network by improving the multi-stream convolutional attention module, and achieved good results on the Ninapro DB1 dataset [31]. Wei et al. explored muscle-gesture correlations and proposed a two-stage multi-stream CNN framework for gesture recognition based on sEMG [32].

However, the application of sEMG faces challenges and issues including the impact of factors such as skin impedance, electrode positioning, and motion artifacts on signal quality. The nonlinear and non-stationary characteristics of sEMG require consideration during signal processing and analysis. Therefore, it is imperative to further optimize the sEMG's acquisition and processing methods, as well as explore effective algorithms for feature extraction and classification, to enhance the accuracy and stability of lower limb behavior intention recognition. Additionally, there is a scarcity of available datasets with limited types of behaviors or only partial availability online, while publicly accessible large-scale datasets predominantly focus on hand movements [33–35]. Hence, accurate collection and organization of lower limb behavior intention data are crucial for developing a diverse and comprehensive dataset that facilitates better evaluation and comparison of different prediction models.

Despite achieving high accuracy, current sEMG-based behavioral intent recognition methods have limitations. The development of a lower-limb behavior intention recognition algorithm based on sEMG aims to accurately control assistive robots. However, improvements in real-time performance and accuracy are necessary for human lower limb behavior recognition algorithms. Designing an efficient and high-performance lower limb behavior recognition algorithm poses a challenge. Recent studies have utilized sEMG to develop behavior recognition methods with extremely fast inference speed. For instance, Zhang et al. [36] proposed an sEMG-based real-time gesture recognition network

combined with a feedforward artificial neural network (ANN), with an average inference time of 227.76 milliseconds. Benalcázar et al. [37] proposed a real-time motion pattern recognition method using the envelope information of EMG, which can be completed within 264.49 milliseconds (ms), including sEMG acquisition time of 256 ms, and achieved an accuracy of 89.5%.

We propose an efficient network for identifying lower limb behavioral intentions based on sEMG, consisting of three main parts: data acquisition, feature extraction, and classifier design. For data acquisition, we collected signals from six major muscles in the right lower limbs of ten people. To diversify the types, we collected six lower limb behaviors, including four periodic behaviors (walking, running, going up-stairs, going down-stairs) with obvious periodicity or quasi-periodicity, and two non-periodic behaviors (crossing obstacles, standing still). For feature extraction, meaningful information is extracted from the collected data using signal processing techniques, such as denoising, wavelet transform, and signal normalization. The classifier (i.e., the proposed ERGN) is mainly built from the proposed main building block called Enhanced Residual Gate Block (ERGB), which integrates the Efficient Channel Attention (ECA) [38] mechanism and hard threshold functions, while leveraging the residual structure. Additionally, the Continuous Wavelet Transform (CWT) is employed to transform one-dimensional signals into two-dimensional images that highlight signal features. The resulting two-dimensional data is then translated and divided using a window size of $400 * 280$ with a step size of 3/4 of the window length, and the pictures under the window are saved. Each cropped picture corresponds to a signal duration of 100 ms. Finally, images containing less feature information are filtered out using the memory size threshold method. 80% of these remaining images are used as the training set for the ERGN while the remaining 20% serve as the test set for performance evaluation.

The main contributions are as follows: (1) We collect a variety of lower limb behavior datasets from 6 acquisition channels to verify the effectiveness of human behavior intention recognition based on sEMG. (2) In order to remove noise points in images and improve the performance of the network, the main building block, ERGB, is designed by integrating an attention mechanism and a hard threshold function. (3) Based on the proposed building block, ERGB, an sEMG-based method for human lower limb behavior intention recognition is proposed, which has the characteristics of high accuracy and high efficiency-outperforming the state-of-the-art research significantly.

2 Sensors and sEMG Acquisition

In this section, we describe the acquisition and processing of surface EMG signals in detail. The sensor device for lower limb sEMG acquisition is presented in Section 2.1. Then, the procedure for lower limb sEMG acquisition is illustrated in Section 2.2. Finally, the preprocessing of the acquired signals is elaborated in Section 2.3.

2.1 Sensors and Preparations

Fig. 1 shows the sensor used for the acquisition of the lower limb sEMG. The sensor is an active induction electromyographic sensor, SEN0240, jointly launched by the DFRobot and the OYMotion. It has the capability to amplify weak human body sEMG signals within the range of ± 1.5 mV by a factor of 1000. The sensor reflects the activity state of human muscles by measuring sEMG of the human body. The amplitude of its output signal exhibits a positive correlation with muscle activity, and its waveform effectively reflects subcutaneous muscle conditions at specific locations. Data generated by human motion is captured by the NI (National Instruments) USB-621x data acquisition (DAQ) devices in conjunction with the NI-DAQmx software to rapidly acquire and display measurements from the DAQ device.

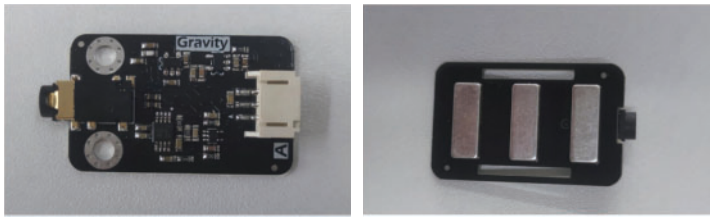

(a) (b)

Figure 1: (a) The myoelectric sensor signal processing board. (b) The metal dry electrode board of the myoelectric sensor

As the selected EMG sensor requires a regulated direct current power supply voltage, we opt for two 4.2 V lithium batteries in series to provide the necessary voltage. To power the sensors and facilitate sEMG collection, we developed a circuit board with a three-terminal voltage regulator that maintains an input voltage range (between 3.3 V and 5.5 V) for the EMG sensor. Fig. 2 displays its printed circuit board (PCB) schematic diagram and physical map. Additionally, this circuit board serves as an overall connection between the multiple myoelectric sensors and the data acquisition equipment, making the data acquisition process easier to control. The left side of this circuit board shown in Fig. 2 is dedicated to connecting the multiple myoelectric sensors, while the right side connects with the USB-621x data acquisition device interface.

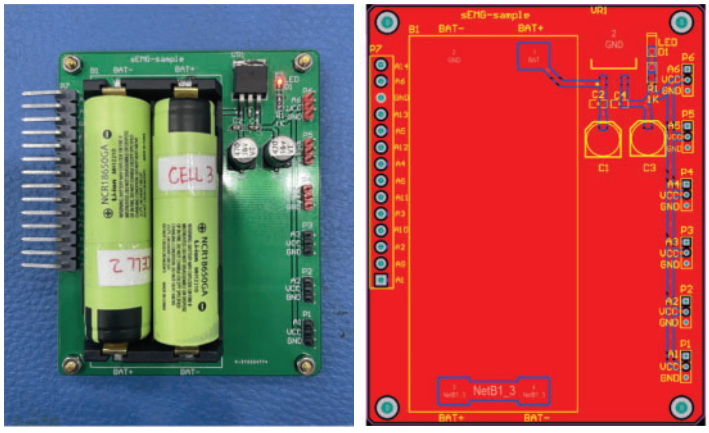

(a) (b)

Figure 2: The developed circuit board. (a) Physical map. (b) PCB schematic. Its right side the connection interface of the multiple myoelectric sensors, and the left side is the connection interface of the data acquisition device USB-621x

The overall connection diagram between multiple devices and human lower limbs when using a single acquisition channel is shown in Fig. 3. Detailed technical specifications for the signal processing board and the dry electrode board can be found in Tables 1 and 2, respectively. As depicted in Figs. 1 and 3, the signal processing board of the myoelectric sensor is connected to the metal dry electrode board via connecting wires. The signal processing board is connected to the corresponding interface in the designed circuit board via using 3P analog signal lines, and the metal dry electrode board is fixed on the selected lower limb muscles by straps. The circuit board is connected to the data acquisition equipment to achieve the capture and fast acquisition of signal data.

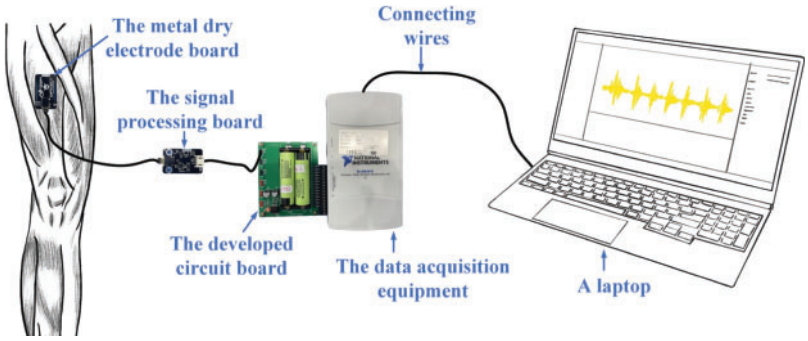

Figure 3: Overall connection diagram between the multiple devices and human lower limbs in the case of a single acquisition channel. The developed circuit board powers the myoelectric sensor while enabling the integral connection of both multiple myoelectric sensors and data acquisition equipment

Table 1: Technical specifications of the signal processing board

Parameter	Power supply voltage	Working voltage	Detection range	Electrode interface	Module interface	Output range	Board size
Data	+3.3 V∼5.5 V	+3.0 V	+/−1.5 mV	PJ-342	PH2.0-3P	0∼3.0 V	22 ∗ 35 mm

Table 2: Technical specifications of the dry electrode board

Parameter	Electrode interface	Electrode wire length	Board size
Data	PJ-342	50 cm	22 ∗ 35 mm

2.2 sEMG Acquisition

Based on the anatomical knowledge of human lower limb muscles and related research [39], we selected 6 muscles highly involved in common lower limb behaviors: rectus femoris (RF) on the front side of the thigh, vastus lateralis (VL), semitendinosus (ST) at the back of the thigh, tibialis anterior (AT), peroneus longus (PL) and gastrocnemius (GM) at the calf. Table 3 displays these six muscles along with their main functions and corresponding acquisition channel serial numbers for each muscle. When collecting sEMG, the metal dry electrode plate is kept in the same direction as the muscle. Fig. 4 illustrates the location of these selected muscles and the proper sensor placement.

Ten healthy subjects participated in this study-four females and six males - performing six types of actions: walking, running, going up stairs, going down stairs, crossing obstacles, and standing still. Before signal collection begin, we wipe clean the skin surfaces where electrodes are placed with alcohol to reduce the influence from oil or sweat on collected signals. Since the EMG sensor module, SEN0240, requires an effective sampling frequency not less than 1000 Hz for sampling, we set the sampling frequency as 1500 Hz. Each subject is asked to perform each action 10 times repeatedly for fifteen seconds each time, and rest for thirty seconds after two repetitions. The data collected during each action execution process represents a set of signal data. Fig. 5 illustrates the six actions. Walking and running on a treadmill with speeds set at 3 and 6.5 km/h, respectively. Performing up and down stairs

requires uniform speed movements between the first and second floors, consisting of a total of 20 steps. Using 8 dumbbells simulate obstacles placed at approximately every normal stride distance (70 ± 10 cm). Each subject crosses over a simulated obstacle in approximately two seconds, and all eight simulated obstacles are crossed, resulting in a complete set of data. For standing still, each subject is asked to stand still for 15 s after resting.

Table 3: The six selected muscles along with their main functions and corresponding acquisition channel serial numbers for each muscle

Acquisition channel serial number	Muscle name	Main functions
1	RF	Extend thighs, bend calves, maintain an upright position
2	VL	Hip flexion and knee extension
3	ST	Extend hip joint, bend knee joint and slightly rotate inward
4	AT	Make the foot dorsiflexion, adduction, and varus
5	PL	Make the foot valgus and plantar flexion
6	GM	Bend the lower leg at the knee joint to synergistically maintain the upright posture of the human body

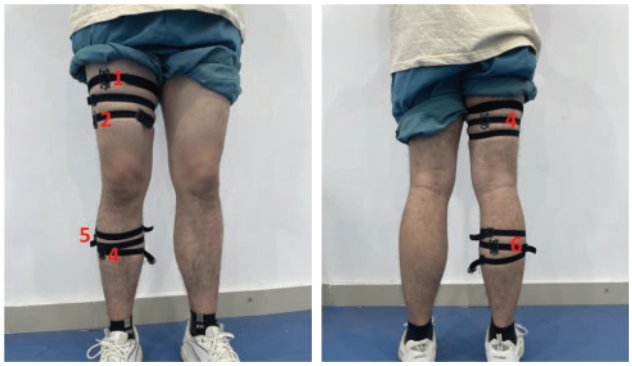

(a) (b)

Figure 4: (a) The frontal view of the sensor placed on the right leg during data collection. (b) The back view of the sensor placed on the right leg during data collection

2.3 Signal Data Preprocessing

The original signal collected is prone to noise interference, thus denoising is necessary as an initial processing step. The sEMG's effective spectrum range is 20 Hz∼500 Hz, which contains meaningful information that can be extracted using a band-pass filter. Power frequency interference (50 Hz) often occurs when collecting weak bioelectrical signals, such as myoelectric signals, electrocardiogram (ECG) signals, and electroencephalogram (EEG) signals. Noise damages the quality of signals and affects the training effect of networks. Common filtering methods include Infinite impulse response (IIR), Butterworth and Finite impulse response (FIR) filters. Their impact on the ERGN predicted results is experimentally compared, and based on the experimental results, we select the FIR filter, as

detailed in the Section 4.4. Fig. 6 illustrates the comparison of the signal before and after filtering with the FIR filter clearly showing its significant effect in removing power frequency dryness. The filtered signal appears smoother and more regular than the original one. Mathematically, the FIR filters are represented as:

$$y(n) = \sum_{t=0}^{M-1} h(t)\, x(n-t) \tag{1}$$

where $x(n)$ is the input signal, $y(n)$ is the output signal, $h(t)$ is the impulse response of the filter, and M is the order of the filter, which is set as 101 in the experiments.

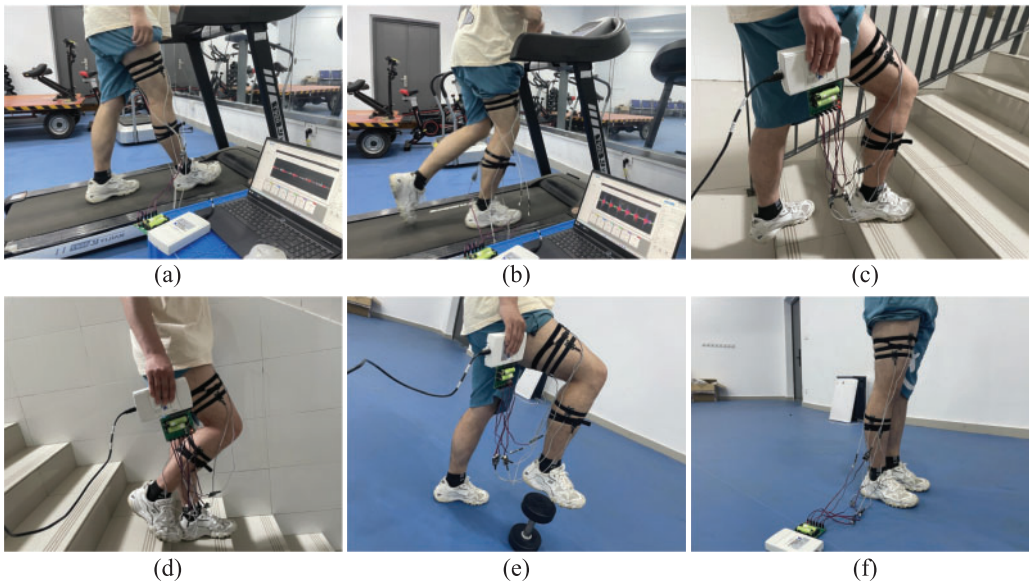

Figure 5: The six common behaviors of the lower limbs selected during data collection. (a) walking, (b) running, (c) going up stairs, (d) going down stairs, (e) crossing obstacles, and (f) standing still

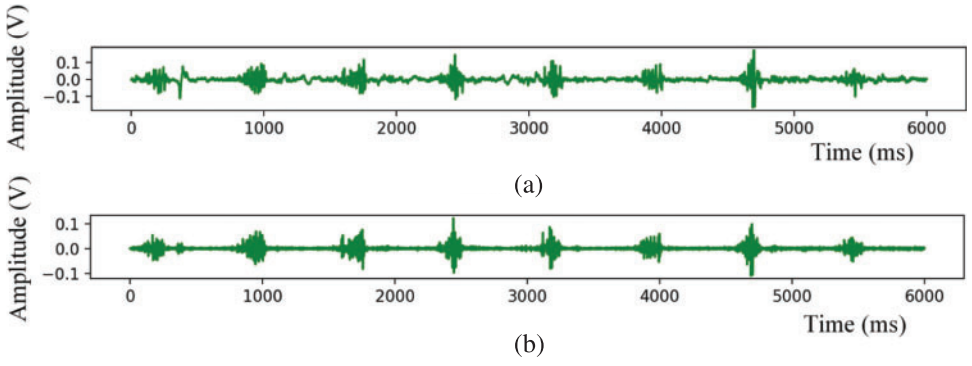

Figure 6: Comparison between the original signal and the signal filtered by the FIR filter. (a) The original signal. (b) The signal after filtering the power frequency interference. The FIR filter has a remarkable filtering effect on the power frequency interference

For extracting the signal features, we opt for using the CWT to extract time-frequency characteristics from sEMG. In signal processing techniques, Fourier transform, short-time Fourier transform (STFT) and wavelet transform are commonly employed. Fourier transform can achieve very high frequency resolution, but it lacks temporal resolution. The latter two provide certain resolutions in both the time and frequency domains, but due to the Heisenberg uncertainty principle, STFT cannot simultaneously achieve high resolution in both frequency and time domains. On the other hand, wavelet transform can accomplish this task effectively while also outperforming the former two methods when dealing with non-stationary signals. Based on this analysis, the wavelet transform is considered the optimal choice for analyzing sEMG signals. Mathematically, the CWT can be expressed as:

$$W_f(a,b) = \frac{1}{\sqrt{|a|}} \int_{-\infty}^{\infty} f(t)\, \psi^* \left(\frac{t-b}{a} \right) dt \tag{2}$$

where $f(t)$ is the signal, $\psi(t)$ is the wavelet basis function, $\psi*(t)$ represents the complex conjugate of the wavelet basis function $\psi(t)$, and $a > 0$ ($a \in R+$) and b ($b \in R$) are scale and translation factors, respectively.

The sEMG results during walking and climbing stairs after CWT processing are presented in Figs. 7 and 8, respectively. Each figure consists of two distinct subfigures, each containing 500 ms of the sEMG information. The color brightness and darkness within the figures represent the amplitude strength and weakness of the signal. Acquisition channels 1 to 6 are displayed from top to bottom. It is evident that there exist significant disparities in muscle participation in the same lower limb behaviors while also observing notable distinctions in muscle activity states across different lower limb behaviors.

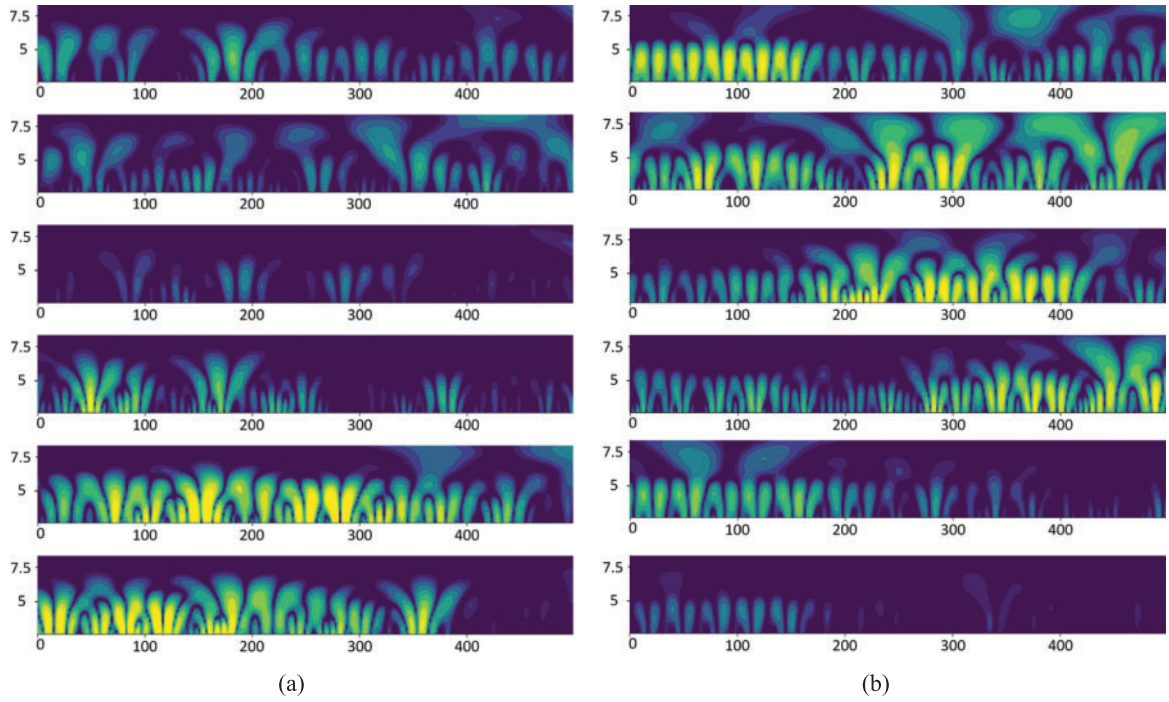

Figure 7: The results of the six acquisition channels sEMG after CWT when walking. (a) and (b) represent the muscles' states in different 500 ms, respectively. From top to bottom are the results of collecting channels 1 to 6

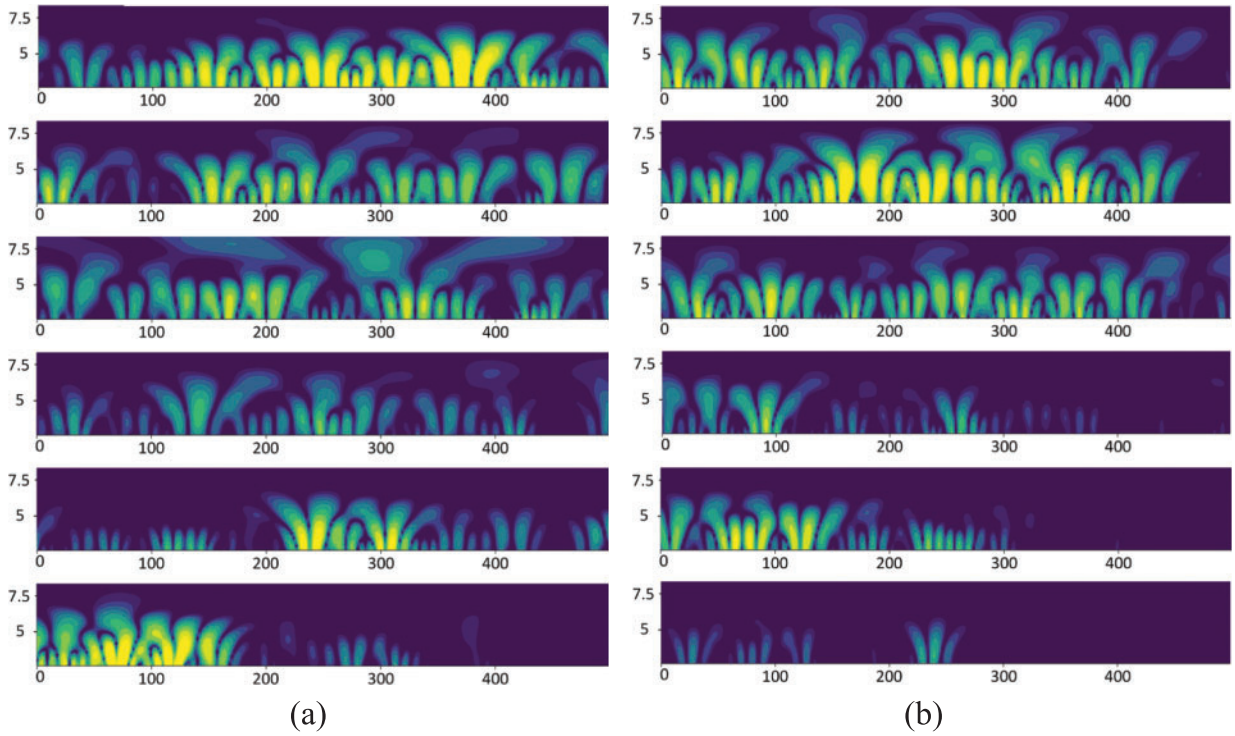

Figure 8: The results of the six acquisition channels sEMG after CWT when going up stairs. (a) and (b) represent the muscles' states in different 500 ms, respectively. From top to bottom are the results of collecting channels 1 to 6

After undergoing CWT processing, the signals are converted into 2D images. The shift window segmentation method is used for data preprocessing, with a window size of $400 * 280$ and a step size of 3/4 of the window length. Each cropped picture corresponds to a signal duration of 100 ms. However, the amount of information contained in the obtained images are uneven, and not every image contains sufficient information for behavioral intention prediction. These images must be filtered out as they can interfere with model learning and judgment during the training or testing processes. It is observed that the memory size occupied by the image is positively correlated with the amount of information contained. We implement a memory size threshold method and set the threshold to 11 kb. If the memory size occupied by the image is less than this threshold, the image will be deleted, and if not, the image will be retained.

3 Methods

3.1 Design of Enhanced Residual Gate Block

3.1.1 Efficient Channel Attention Mechanism

In order to enhance the effectiveness of feature learning, the channel attention mechanism, Efficient Channel Attention (ECA), is introduced into the network. The ECA attention mechanism has the advantage of having fewer parameters, which can improve the model efficiency. This is crucial for the application of lower limb behavior intention detection models based on sEMG. As depicted in Fig. 9, the ECA effectively facilitates cross-channel information exchange, and its implementation process is as follows: (1) The input feature map undergoes global average pooling (GAP), transforming

it from a matrix of $C * W * H$ to a vector of $C * 1 * 1$; (2) The adaptive one-dimensional convolution kernel size k is calculated based on the number of channels in the feature map; (3) Apply the k to one-dimensional convolution to obtain the weights for each channel of the feature map. Specifically,

$$y_i = GAP(d_i), d_i \in P \tag{3}$$

where P is the set of feature vector channels that need to be weighted, d_i is the feature vector channel of the i-th layer in P, y_i is the feature matrix of d_i obtained by GAP operation. The formula for the local weighted weight, ω_i, of the channel is as follows:

$$\omega_i = Sigmoid\left(\sum_{j=1}^{k} \alpha^j y_i^j\right), y_i^j \in \Omega_i^j \tag{4}$$

where $Sigmoid$ is the sigmoid activation function, Ω_i^j is the set of k adjacent feature channels of y_i, α is the initial value of the j-th channel, and y_i^j is the output value of the j-th channel adjacent to the i-th feature vector channel. The channel attention weight, ω, is represented as follows:

$$\omega = Sigmoid(Conv1D(y)) \tag{5}$$

where y represents the aggregation feature, and $Conv1D$ represents the one-dimensional convolution operation. There is a mapping relationship ϕ between the value of kernel k in 1D convolution and the channel dimension C:

$$C = \phi(k) \tag{6}$$

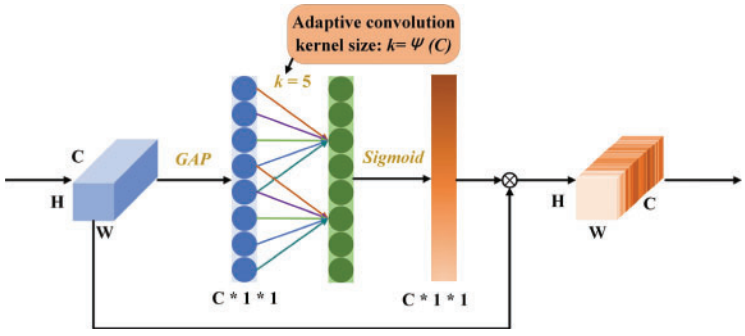

Figure 9: The ECA attention mechanism. The GAP represents the global average pooling, while the $Sigmoid$ represents the sigmoid activation function

The simplest mapping method is to use a linear function, i.e., $\varphi(k) = \gamma * k - b$, but its linearity has limitations. The channel dimension C (the number of convolutional kernels) is usually chosen to the nth power of 2. Therefore, this mapping function can be extended to the following nonlinear functions:

$$C = \phi(k) = 2^{(\gamma * k - b)} \tag{7}$$

Subsequently, the convolutional kernel size k can be expressed as:

$$k = \psi(C) = \left|\frac{\log_2(C)}{\gamma} + \frac{b}{\gamma}\right|_{odd} \tag{8}$$

where $|t|_{odd}$ represents the odd number closest to t. Based on experience, b and γ are set to 1 and 2, respectively.

3.1.2 Gate Function

Deep Residual Shrinkage Network (DRSN) [40] integrates squeeze-and-excitation networks (SENet) with a soft threshold function derived from traditional signal denoising methods while leveraging deep residual networks' learning advantages. The main building block, Residual shrinkage building unit (RSBU), reduces unnecessary features in signals and automatically learns thresholds based on input signals characteristics. The RSBU is developed upon architectural principles of Residual building unit (RBU) [41]. The difference is that the RSBU embeds a soft threshold function module to reduce the impact of noise on networks' performance compared with the RBU. The clear explanation of this soft threshold function is as follows:

$$x_{out} = \begin{cases} x_{in} - \tau & x_{in} > \tau \\ 0 & -\tau \leq x_{in} \leq \tau \\ x_{in} + \tau & x_{in} < -\tau \end{cases} \tag{9}$$

where x_{in}, x_{out} and τ represent input data, output data and threshold, respectively. The soft thresholding is commonly employed in signal processing tasks to reduce noise by shrinking data towards zero. It is implemented as a shrinkage layer in the DRSN eliminating irrelevant features by setting them to zero. However, it should be noted that this operation may also weaken meaningful features, thereby affecting networks' performance. The soft thresholding is at the heart of the building block RSBU and must be carefully considered accordingly. Based on the above considerations, the hard threshold function, as gate function of the building blocks ERGB, is used in images processing for noise removal and enhancing images clarity. This hard threshold function serves as an enhancement layer in the proposed ERGB and can be formally expressed as:

$$x_{out} = \begin{cases} x_{in} & x_{in} > \tau \\ 0 & -\tau \leq x_{in} \leq \tau \\ x_{in} & x_{in} < -\tau \end{cases} \tag{10}$$

We incorporate the ECA and the gate function (Eq. 10) into the proposed ERGB. The ECA enhances the network's performance by adjusting channel weights adaptively without increasing complexity. The gate function effectively denoises signals and highlights informative features. Fig. 10 illustrates the architecture of the ERGB, with the gate function inside the dashed box.

3.2 Design of Enhanced Residual Gate Network

We employ the ERGB to construct a network, ERGN, for recognizing lower limb behavioral intentions. Overall, the ERGN adopts a residual structure to compensate for feature degradation caused by deep network architecture. It incorporates multiple the ERGB and establishes residual connections between the output of the first convolutional layer and the final ERGB output, as illustrated in Fig. 11. The multiple acquisition channels are fused together as input for the proposed ERGN. Towards the end of the ERGN, only a GAP layer is utilized to aggregate and average all values of each channel in the signal feature map, resulting in a feature vector that is directly employed for classifying lower limb behavioral intentions.

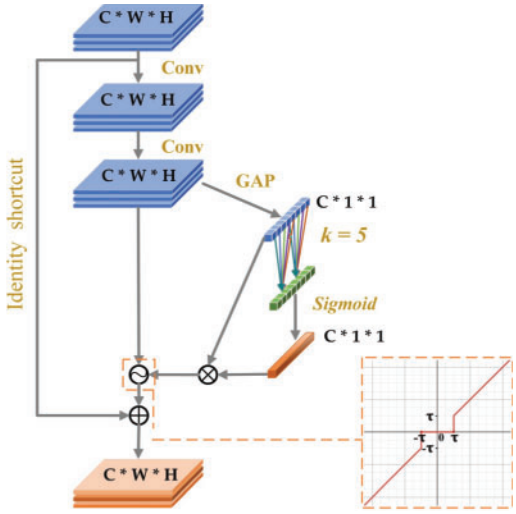

Figure 10: The architecture of the main building blocks, ERGB. The *GAP*, *Sigmoid* and *Conv* represent the global average pooling, the sigmoid activation function and the convolution, respectively

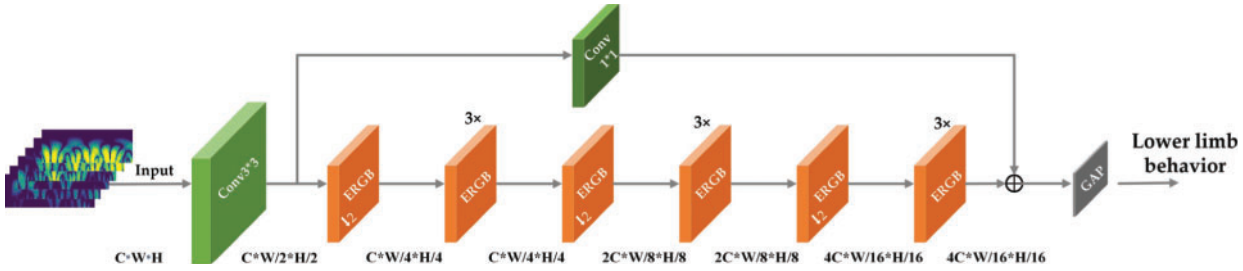

Figure 11: The network architecture of the proposed ERGN

4 Results and Analysis

4.1 Evaluation Methods

In order to investigate the impact of various factors on the proposed ERGN's performance, such as muscles combinations, hard threshold functions and wavelet functions, we employ common evaluation methods. The accuracy is an effective evaluation metric, and both its maximum value and average value will be utilized as measures of the model. To comprehensively demonstrate the network performance, the F1-score is introduced to consider precision and recall capabilities of the model. They can be formally expressed as:

$$Accuracy = \frac{TP + TN}{TP + FP + TN + FN} \tag{11}$$

$$F1 - score = \frac{2 \times Presion \times Recall}{Presion + Recall} \tag{12}$$

where TP, FP, TN, and FN are True Positive, False Positive, True Negative, and False Negative, respectively. The precision and recall can be expressed as:

$$Precision = \frac{TP}{TP + FP} \tag{13}$$

$$Recall = \frac{TP}{TP + FN} \tag{14}$$

4.2 Different Combinations of sEMG Acquisition Channels

We select six muscles that are highly involved in common lower body behaviors to collect signals. Fig. 12 displays the signal data of six acquisition channels for each lower limb behavior. A metal dry electrode plate is fixed on a muscle, which serves as an acquisition channel. It can be seen from Fig. 12 that there are significant differences in the involvement of the six selected muscles for different lower limb behaviors. Under the same network and configuration, we conduct experiments to investigate whether combining different acquisition channel data has a significant impact on the network's recognition of lower limb behavior-specifically, which muscle combinations can more accurately represent a certain lower limb behavior. Given the wide variety of daily life's lower limb behaviors, we only considered the combinations of five and six acquisition channels without considering fewer ones.

The results of this experiment are presented in Table 4. It can be observed that the sixth combination yields optimal results with a maximum accuracy rate of 98.41%, an average accuracy rate of 98.02%, and an F1-score of 0.994, which outperform all other input combinations listed in Table 4 including using all six acquisition channels as input. This is because many unconscious or irrelevant actions may occur during performing lower limb behaviors leading to network's misjudgment. Therefore, selecting fewer muscles when collecting data does not necessarily result in worse performance outcomes as demonstrated by our findings.

4.3 Hard Threshold Function

The proposed ERGB utilizes the hard threshold function as a gate function to eliminate noise points and enhance image quality. To investigate the impact of threshold function on the ERGN's performance, we conduct ablation experiments, and the results are presented in Table 5. The experimental results demonstrate that using threshold functions can improve the network performance significantly. Furthermore, compared to the soft threshold function, utilizing the hard threshold function in the proposed ERGN leads to a remarkable increase in accuracy.

4.4 Selection of the Filter

The acquisition of signals is susceptible to interference from the 50 Hz power frequency. Common filtering techniques include the IIR, Butterworth and FIR filters. The impact of the signals processed by the three on the performance of the proposed ERGN is shown in Table 6. Experimental results indicate that there are relatively minor differences among these filters in terms of their effect on signal processing for this model. Based on the data presented in Table 6, the FIR filter is selected to eliminate power frequency noise.

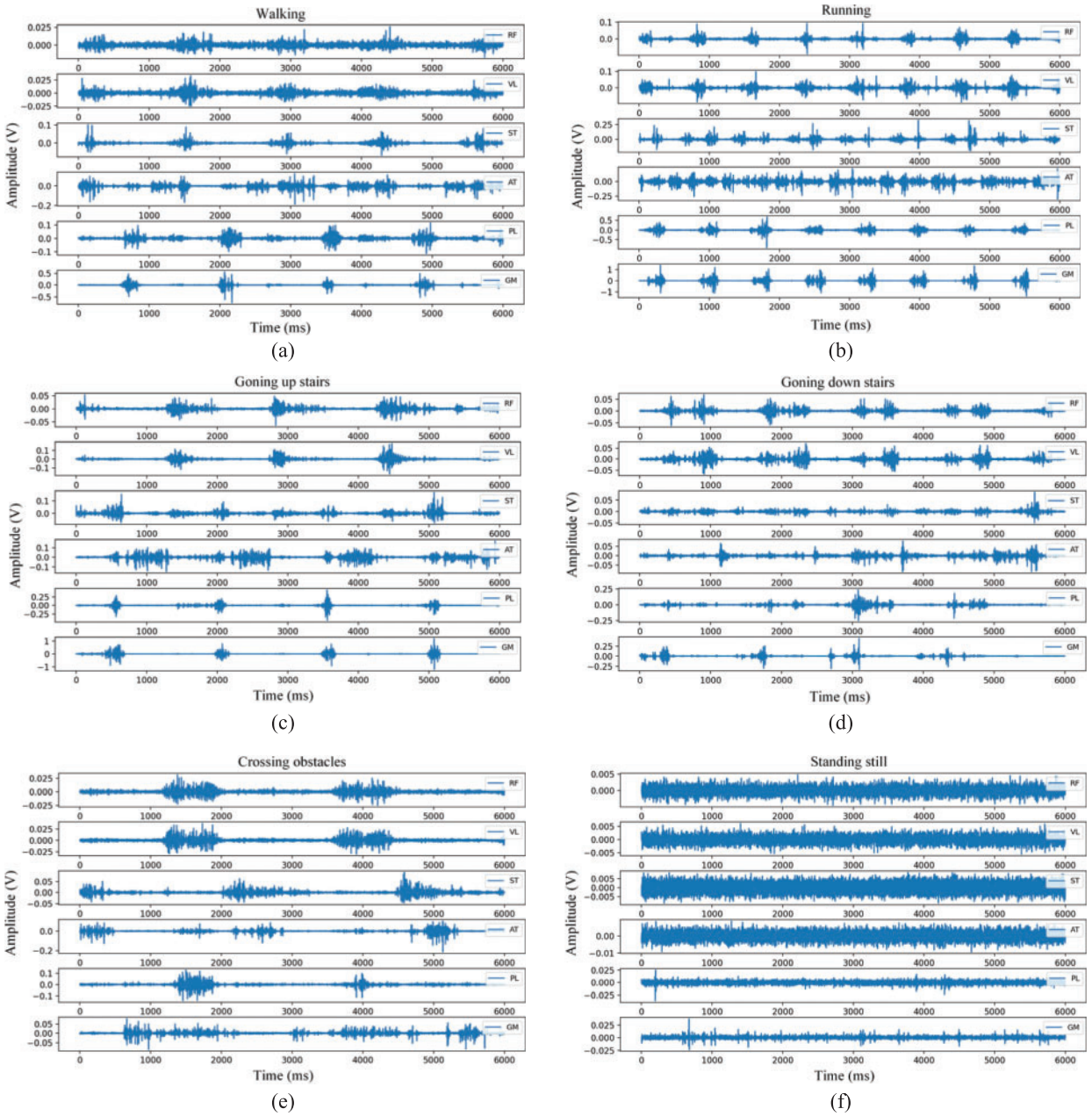

Figure 12: The sEMG of 6 acquisition channels for different lower limb behaviors. The magnitude of the signal amplitude reveals the degree of muscle engagement

4.5 Different Wavelet Functions

In the data preprocessing task, we apply the CWT to sEMG to convert the one-dimensional signal into two-dimensional data and obtain images encompassing both temporal and frequency information of original signals. The CWT can decompose the signal into different frequency components, and the selection of the wavelet function is the key point of applying the CWT. We conduct comparative

experiments on common wavelet functions in the CWT, namely Mexican Hat, Paul and Morlet. Fig. 13 visualizes the processed signals using these three wavelet functions. The results presented in Table 7 demonstrate the impact of using different wavelet functions on the final classification performance of the proposed ERGN. It can be seen that Mexican Hat as the wavelet function yields superior network performance, achieving both the highest accuracy and F1-score.

Table 4: The effects of different combinations of sEMG acquisition channels on the classification performance of the proposed ERGN in predicting lower limb behavior intentions

sEMG acquisition channels						Max accuracy	Ave accuracy	F1-score
1	2	3	4	5	6			
√	√	√	√	√	√	97.35%	96.84%	0.980
	√	√	√	√	√	95.55%	95.01%	0.954
√		√	√	√	√	97.64%	97.24%	0.985
√	√		√	√	√	97.01%	96.46%	0.975
√	√	√		√	√	95.05%	94.36%	0.941
√	√	√	√		√	98.41%	98.02%	0.994
√	√	√	√	√		96.57%	96.04%	0.971

Table 5: The max accuracy of the proposed ERGN in predicting lower limb behavioral intentions under the utilization of threshold functions

sEMG acquisition channels						Use the soft threshold function	Use the hard threshold function	Not use threshold functions
1	2	3	4	5	6			
√	√	√	√	√	√	96.01%	97.35%	93.05%
	√	√	√	√	√	93.74%	95.55%	90.41%
√		√	√	√	√	95.98%	97.64%	93.60%
√	√		√	√	√	95.67%	97.01%	94.15%
√	√	√		√	√	93.11%	95.05%	90.98%
√	√	√	√		√	96.67%	98.41%	94.18%
√	√	√	√	√		94.98%	96.57%	93.64%

4.6 Inference Time

The signal duration corresponding to the information contained in each segmented picture is 100 ms through the shifting window segmentation. The corresponding network inference time is 20 ms. Since sEMG are generally generated 30–150 ms prior to limb movement, the proposed ERGN has the ability to recognize lower limb behavior in real time, reflecting its high efficiency.

Table 6: The influence of signals processed by the IIR, Butterworth and FIR filters on the performance of the proposed ERGN

	IIR filter	Butterworth filter	FIR filter
Max accuracy	98.35%	98.39%	98.41%
Avg accuracy	97.98%	98.03%	98.02%
F1-score	0.990	0.992	0.994

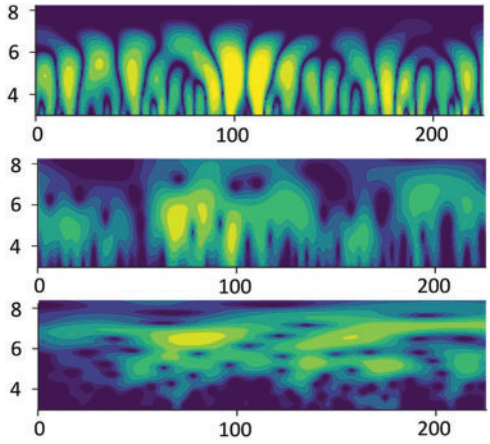

Figure 13: Visualization of the signal after CWT processing using these three wavelet functions. From top to bottom are the results when the wavelet functions are the MexicanHat, Paul and Morlet, respectively

Table 7: The influence of different wavelet functions on the proposed ERGN's classification performance

	Selection of wavelet functions		
	MexicanHat	Paul	Morlet
Max accuracy	98.41%	98.19%	97.20%
Avg accuracy	98.02%	97.73%	96.31%
F1-score	0.994	0.988	0.974

4.7 Robustness Testing

sEMG may be affected by the environment and sensors (electrodes) due to its high sensitivity, resulting in noise and occasional sudden changes. Considering these factors, we conduct the robustness testing on the proposed ERGN. The testing methods include: (a) introducing the Gaussian white noise to the sEMG; (b) inducing the Salt-and-pepper noise in the sEMG to simulate occasional sudden change. Under these circumstances, we evaluate the performance of the ERGN and present the experimental results in Table 8. Without any added the noise (before (a) and (b)) or with only the Gaussian white noise, the ERGN has excellent performance with an accuracy above 98%. However,

when the abnormal signals with sudden changes appear in signals, it significantly affects the model's accuracy. This is evident from the last two rows of Table 8.

Table 8: The robustness testing on the proposed ERGN

	Max accuracy	Ave accuracy
Before (a) and (b)	98.41%	98.02%
(a)	98.01%	97.34%
(b)	95.87%	94.98%
(a) + (b)	95.05%	94.33%

4.8 Comparing Experimental Results

To demonstrate the advantages of the proposed ERGN, we conduct a comparative analysis with state-of-the-art (SOTA) networks. Table 9 presents the experiments' results, clearly demonstrating that the ERGN outperforms all other models in terms of the maximum accuracy (98.41%), average accuracy (98.02%), and F1-score (0.994). The maximum and average accuracies of most networks are below 90%, and the F1-scores are below 0.900. The accuracy of the second best performing DRSN-CW is about 6% lower and the F1-score value is about 0.1 lower than the proposed ERGN.

Table 9: The comparison results between the proposed ERGN and the SOAT networks

	Max accuracy	Ave accuracy	F1-score
MCBAM-GRU [31]	86.92%	86.09%	0.870
2SRNN [42]	86.33%	85.65%	0.859
MSITL [43]	84.96%	84.11%	0.822
DRSN-CW [40]	92.80%	92.03%	0.906
MSFFusionNet [32]	83.57%	82.46%	0.808
ERGN (ours)	98.41%	98.02%	0.994

5 Conclusion

Combining an attention mechanism, a hard threshold function and a residual network, we propose a building block, ERGB, and an sEMG-based efficient network, ERGN, for lower limb behavior intention recognition. We utilize the CWT to perform two-dimensional processing on the signal while integrating the time-frequency characteristics of a signal. Crop, segment, and filter the obtained images, and use multiple acquisition channels as inputs for the proposed ERGN. The experimental results demonstrate the effectiveness of the hard threshold function and the high accuracy and efficiency of the proposed ERGN. However, further efforts are required to improve model's robustness. An undeniable phenomenon is that the sEMG is susceptible to interference due to its high sensitivity, which can cause abnormal signals in sEMG leading to interfere with actual application of the existing relevant models. In future research, we will study fault-tolerant mechanisms that identify these abnormal signals and reconstruct them to enhance models' robustness.

Acknowledgement: The authors are grateful to all the members of the lower limb exoskeleton rehabilitation training robot research team of the School of Artificial Intelligence of Anhui University of Science and Technology for their advice and help in this study.

Funding Statement: The Research and the Development Fund of the Institute of Environmental Friendly Materials and Occupational Health, Anhui University of Science and Technology, Grant/Award Number: ALW2022YF06; Academic Support Project for Top-Notch Talents in Disciplines (Majors) of Colleges and Universities in Anhui Province, Grant/Award Number: gxbjZD2021052; The University Synergy Innovation Program of Anhui Province, Grant/Award Number: GXXT-2022-053; Anhui Province Key R&D Program of China, Grant/Award Number: 2022i01020015.

Author Contributions: Study conception and design: Liuyi Ling, Yiwen Wang, Fan Ding; writing-original draft: Liuyi Ling, Yiwen Wang; methodology: Liuyi Ling, Yiwen Wang; writing-review & editing: Fan Ding, Li Jin; data curation: Li Jin, Bin Feng; validation: Fan Ding, Weixiao Li, Chengjun Wang; project administration: Chengjun Wang, Xianhua Li. All authors reviewed the results and approved the final version of the manuscript.

Availability of Data and Materials: The data that support the findings of this study are available on request from the corresponding author. The data are not publicly available due to privacy or ethical restrictions.

Conflicts of Interest: The authors declare that they have no conflicts of interest to report regarding the present study.

References

[1] P. Shamli Fathima, C. Sandhra, D. Jojo, A. V. Gayathri, N. Sidharth *et al.,* "Fatigue analysis of biceps brachii muscle using sEMG signal," *Smart Sensors Measurements and Instrumentation*, vol. 750, pp. 307–314, 2021.

[2] R. Merletti, I. Campanini, W. Z. Rymer and C. Disselhorst-Klug, "Editorial: Surface electromyography: Barriers limiting widespread use of sEMG in clinical assessment and neurorehabilitation," *Frontiers in Neurology*, vol. 12, pp. 642257, 2021.

[3] Y. Luan, Y. Shi, W. Wu, Z. Liu, H. Chang *et al.,* "HAR-sEMG: A dataset for human activity recognition on lower-limb sEMG," *Knowledge and Information Systems*, vol. 63, no. 10, pp. 2791–2814, 2021.

[4] G. Yang, M. Jiang, W. Ouyang, G. Ji, H. Xie *et al.,* "IoT-based remote pain monitoring system: From device to cloud platform," *IEEE Journal of Biomedical and Health Informatics*, vol. 22, no. 6, pp. 1711–1719, 2018.

[5] S. Kwon and J. Kim, "Real-time upper limb motion estimation from surface electromyography and joint angular velocities using an artificial neural network for human-machine cooperation," *IEEE Transactions on Information Technology in Biomedicine*, vol. 15, no. 4, pp. 522–530, 2011.

[6] C. Liu, X. Chu, W. Wu, S. Li, Z. He *et al.,* "Human-machine cooperation research for navigation of maritime autonomous surface ships: A review and consideration," *Ocean Engineering*, vol. 246, pp. 110555, 2022.

[7] M. F. Montoya, J. E. Muñoz and O. A. Henao, "Enhancing virtual rehabilitation in upper limbs with biocybernetic adaptation: The effects of virtual reality on perceived muscle fatigue, game performance and user experience," *IEEE Transactions on Neural Systems and Rehabilitation Engineering*, vol. 28, no. 3, pp. 740–747, 2020.

[8] A. Dash and U. Lahiri, "Design of virtual reality-enabled surface electromyogram-triggered grip exercise platform," *IEEE Transactions on Neural Systems and Rehabilitation Engineering*, vol. 28, no. 2, pp. 444–452, 2019.
[9] J. Huang, Z. Li, H. Xia, G. Chen and Q. Meng, "Cross-modal integration and transfer learning using fuzzy logic techniques for intelligent upper limb prosthesis," *IEEE Transactions on Fuzzy Systems*, vol. 31, no. 4, pp. 1267–1280, 2023.
[10] D. Xu and Q. Wang, "Noninvasive human-prosthesis interfaces for locomotion intent recognition: A review," *Cyborg and Bionic Systems*, vol. 2021, no. 3, pp. 466, 2021. https://doi.org/10.34133/2021/9863761
[11] Y. H. Byeon, S. B. Pan and K. C. Kwak, "Intelligent deep models based on scalograms of electrocardiogram signals for biometrics," *Sensors*, vol. 19, no. 4, pp. 935, 2019. https://doi.org/10.3390/s19040935
[12] L. Bi, S. Xia and W. Fei, "Hierarchical decoding model of upper limb movement intention from EEG signals based on attention state estimation," *IEEE Transactions on Neural Systems and Rehabilitation Engineering*, vol. 29, pp. 2008–2016, 2021.
[13] X. Li, Y. Zheng, Y. Liu, L. Tian, P. Fang *et al.,* "A novel motion recognition method based on force myography of dynamic muscle contractions," *Frontiers in Neuroscience*, vol. 15, pp. 783539, 2022. https://doi.org/10.3389/fnins.2021.783539
[14] J. W. Cui, H. Du, B. F. Yan and X. J. Wang, "Research on upper limb action intention recognition method based on fusion of posture information and visual information," *Electronics*, vol. 11, no. 19, pp. 3078, 2022.
[15] P. Huang, H. Wang, Y. Wang, Y. Geng, W. Yu *et al.,* "*In-situ* measuring sEMG and muscle shape change with a flexible and stretchable hybrid sensor for hand gesture recognition," *IEEE Transactions on Neural Systems and Rehabilitation Engineering*, vol. 31, pp. 581–592, 2023.
[16] S. Kyeong, J. Feng, J. K. Ryu, J. J. Park, K. H. Lee *et al.,* "Surface electromyography characteristics for motion intention recognition and implementation issues in lower-limb exoskeletons," *International Journal of Control, Automation and Systems*, vol. 20, no. 3, pp. 1018–1028, 2022.
[17] R. Abdollahpoor and N. Lotfivand, "Fully adaptive denoising of ECG signals using empirical mode decomposition with the modified indirect subtraction and the adaptive window techniques," *Circuits Systems, and Signal Processing*, vol. 39, no. 8, pp. 4021–4046, 2020.
[18] X. Zong, F. Wang, J. She and J. Zhao, "Denoising method for surface electromyography signals combining CEEMDAN and interval total variation," *Circuits Systems, and Signal Processing*, vol. 41, no. 11, pp. 6493–6512, 2022.
[19] Y. Li, K. Bai, H. Wang, S. Chen, X. Liu *et al.,* "Research on improved FAWT signal denoising method in evaluation of firefighter training efficacy based on sEMG," *Biomedical Signal Processing and Control*, vol. 72, no. 1, pp. 103336, 2022.
[20] R. N. Khushaba, A. H. Al-Timemy, O. W. Samuel and E. J. Scheme, "Myoelectric control with fixed convolution-based time-domain feature extraction: Exploring the spatio-temporal interaction," *IEEE Transactions on Human-Machine Systems*, vol. 52, no. 6, pp. 1247–1257, 2022.
[21] M. Atzori and H. Müller, "PaWFE: Fast signal feature extraction using parallel time windows," *Frontiers in Neurorobotics*, vol. 13, pp. 74, 2019.
[22] P. Xanthopoulos, P. M. Pardalos and T. B. Trafalis, *Robust data mining*. New York, USA: Springer, 2013. [Online]. Available: https://link.springer.com/chapter/10.1007/978-1-4419-9878-1_4
[23] J. Lever, M. Krzywinski and N. Altman, "Principal component analysis," *Nature Methods*, vol. 14, no. 7, pp. 641–642, 2017.
[24] M. Zhu, X. Guan, Z. Li, L. He, Z. Wang *et al.,* "SEMG-based lower limb motion prediction using CNN-LSTM with improved PCA optimization algorithm," *Journal of Bionic Engineering*, vol. 20, no. 2, pp. 612–627, 2023.
[25] W. Song, Q. Han, Z. Lin, N. Yan, D. Lou *et al.,* "Design of a flexible wearable smart sEMG recorder integrated gradient boosting decision tree based hand gesture recognition," *IEEE Transactions on Biomedical Circuits and Systems*, vol. 13, no. 6, pp. 1563–1574, 2019.
[26] P. Qin and X. Shi, "Evaluation of feature extraction and classification for lower limb motion based on sEMG signal," *Entropy*, vol. 22, no. 8, pp. 852, 2020.

[27] J. Zeng, Y. Zhou, Y. Yang, J. Yan and H. Liu, "Fatigue-sensitivity comparison of sEMG and A-mode ultrasound based hand gesture recognition," *IEEE Journal of Biomedical and Health Informatics*, vol. 26, no. 4, pp. 1718–1725, 2022.
[28] S. Hua, C. Wang and X. Wu, "A novel sEMG-based force estimation method using deep-learning algorithm," *Complex & Intelligent Systems*, vol. 8, no. 3, pp. 1949–1961, 2022.
[29] N. Nasri, S. Orts-Escolano and M. Cazorla, "An sEMG-controlled 3D game for rehabilitation therapies: Real-time time hand gesture recognition using deep learning techniques," *Sensors*, vol. 20, no. 22, pp. 6451, 2020.
[30] P. Tsinganos, B. Cornelis, J. Cornelis, B. Jansen and A. Skodras, "Hilbert sEMG data scanning for hand gesture recognition based on deep learning," *Neural Computing and Applications*, vol. 33, no. 7, pp. 2645–2666, 2021.
[31] S. Wang, L. Huang, D. Jiang, Y. Sun, G. Jiang *et al.,* "Improved multi-stream convolutional block attention module for sEMG-based gesture recognition," *Frontiers in Bioengineering and Biotechnology*, vol. 10, pp. 909023, 2022. https://doi.org/10.3389/fbioe.2022.909023
[32] W. Wei, Y. Wong, Y. Du, Y. Hu, M. Kankanhalli *et al.,* "A multi-stream convolutional neural network for sEMG-based gesture recognition in muscle-computer interface," *Pattern Recognition Letters*, vol. 119, no. 1, pp. 131–138, 2019.
[33] N. Gao and L. Zhao, "A pedestrian dead reckoning system using sEMG based on activities recognition," in *2016 IEEE Chinese Guidance, Navigation and Control Conf. (CGNCC)*, Nanjing, China, pp. 2361–2365, 2016.
[34] M. Atzori, A. Gijsberts, S. Heynen, A. M. Hager, O. Deriaz *et al.,* "Building the Ninapro database: A resource for the biorobotics community," in *2012 4th IEEE RAS & EMBS Int. Conf. on Biomedical Robotics and Biomechatronics (BioRob)*, Rome, Italy, pp. 1258–1265, 2012.
[35] C. Sapsanis, "Recognition of basic hand movements using electromyography," Ph.D. dissertation, University of Patras, Greece, 2013.
[36] Z. Zhang, K. Yang, J. Qian and L. Zhang, "Real-time surface EMG pattern recognition for hand gestures based on an artificial neural network," *Sensors*, vol. 19, no. 14, pp. 3170, 2019.
[37] M. E. Benalcázar, C. Motoche, J. A. Zea, A. G. Jaramillo, E. C. Anchundia *et al.,* "Real-time hand gesture recognition using the Myo Armband and muscle activity detection," in *2017 IEEE Second Ecuador Technical Chapters Meeting (ETCM)*, Salinas, Ecuador, pp. 1–6, 2017.
[38] Q. Wang, B. Wu, P. Zhu, P. Li, W. Zuo *et al.,* "ECA-Net: Efficient channel attention for deep convolutional neural networks," in *2020 IEEE/CVF Conf. on Computer Vision and Pattern Recognition (CVPR)*, Seattle, WA, USA, pp. 11531–11539, 2020.
[39] C. Fleischer and G. Hommel, "Calibration of an EMG-based body model with six muscles to control a leg exoskeleton," in *Proc. of 2007 IEEE Int. Conf. on Robotics and Automation*, Rome, Italy, pp. 2514–2519, 2007.
[40] M. Zhao, S. Zhong, X. Fu, B. Tang and M. Pecht, "Deep residual shrinkage networks for fault diagnosis," *IEEE Transactions on Industrial Informatics*, vol. 16, no. 7, pp. 4681–4690, 2020.
[41] K. He, X. Zhang, S. Ren and J. Sun, "Deep residual learning for image recognition," in *2016 IEEE Conf. on Computer Vision and Pattern Recognition (CVPR)*, Las Vegas, NV, USA, pp. 770–778, 2016.
[42] I. Ketykó, F. Kovács and K. Z. Varga, "Domain adaptation for sEMG-based gesture recognition with recurrent neural networks," in *Int. Joint Conf. on Neural Networks (IJCNN)*, Budapest, Hungary, pp. 1–7, 2019.
[43] K. Wang, Y. Chen, Y. Zhang, X. Yang and C. Hu, "Multi-source integration based transfer learning method for cross-user sEMG gesture recognition," in *Int. Joint Conf. on Neural Networks (IJCNN)*, Padua, Italy, pp. 1–8, 2022.